Active control of the depletion boundary layers in microfluidic electrochemical reactors†

Seong Kee Yoon,[a] Geoff W. Fichtl[b] and Paul J. A. Kenis*[b]

Received 30th June 2006, Accepted 23rd August 2006
First published as an Advance Article on the web 14th September 2006
DOI: 10.1039/b609289f

In this paper, we describe three methods to improve the performance of pressure-driven laminar flow-based microreactors by manipulating reaction-depletion boundary layers to overcome mass transfer limitations at reactive surfaces on the walls, such as electrodes. The transport rate of the reactants to the reactive surfaces is enhanced by (*i*) removing the depleted zone through multiple periodically-placed outlets; (*ii*) adding fresh reactants through multiple periodically-placed inlets along the reactive surface; or (*iii*) producing a spiraling, transverse flow through the integration of herringbone ridges along the channel walls. For approaches (*i*) and (*ii*), the network of microfluidic channels needs to be designed such that under the operating conditions used the right amount of boundary layer at each outlet or inlet is removed or replenished, respectively. Here, we report a set of design rules, derived with the help of a fluidic resistance circuit model, to aid in the design of appropriate microfluidic networks. Also, the actual enhancement of the performance of the electrochemical microreactor, *i.e.* chemical conversion efficiency, using multiple inlets, multiple outlets, or herringbone ridges is reported.

Introduction

A common feature of research and development in the area of microchemical systems is accounting for or exploiting the characteristics and transport phenomena of the microscale. The inherently short transport distances imply steeper thermal and concentration gradients, leading to higher heat and mass transfer rates.[1] In addition, shorter residence times can be attained in a microreactor compared to the macroscale, and the inherent high surface-to-volume ratios encountered at the microscale can be exploited in heterogeneous catalysis.[2] Moreover, viscous forces dominate inertial forces in microfluidic channels due to the high surface-to-volume ratios, leading to the occurrence of laminar flow. The absence of turbulence in this laminar flow regime, which is characterized by a Reynolds number Re smaller than 2000, renders diffusion as the sole mechanism for mixing.[3] Over the last decade many microchemical systems comprising microfluidic networks have been created, including micro total analysis systems (μTAS),[4,5] microreactors to perform actual chemical conversions,[6–9] and microfluidic chips as enabling tools for a wide range of biological studies.[10–16] Moreover, a wide range of applications has been developed that exploit laminar flows comprising multiple streams of different chemical composition that proceed to flow laminarly in parallel, for example, in various T- and H-based biosensors[17,18] and in membraneless fuel cells.[19–21]

The performance of microfluidic systems that rely on surface interactions, *i.e.* biochemical reactions (*e.g.* DNA hybridization[22]) and electrochemical reactions (*e.g.* cofactor regeneration,[23] fuel cells[19–21]), is limited by either reaction kinetics or the rate of mass transfer to the reactive surfaces. The primary focus of this paper is to present and analyze multiple options to enhance steady-state diffusion-limited mass transport to a reactive surface under a pressure-driven flow condition, which is known as the Graetz problem.[24] Fig. 1 shows a schematic of a generic multistream laminar flow-based electrochemical microreactor, in which electrochemical reactions take place on electrodes that line opposing, inside walls of a microfluidic channel. The two mass transfer-related physicochemical phenomena that determine the performance of such microreactors are (*i*) slow mixing by interdiffusion of the two streams at the liquid–liquid interface (Fig. 1b) and (*ii*)

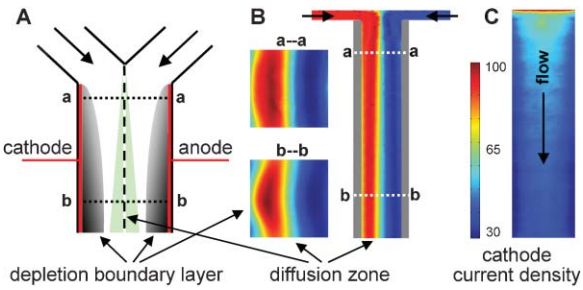

Fig. 1 (A) Schematic representation of a laminar flow-based electrochemical microreactor in which depletion boundary layers form along the length of the electrodes (not to scale). (B) Top view and cross-sectional views of a FEMLAB simulation of such a reactor with a thin depletion layer forming on the left electrode, while diffusional broadening is taking place at the liquid–liquid interface. (C) Frontal view of one of the electrodes, visualizing the extent of reaction (arbitrary units). Most of the reaction occurs at the onset of the electrode at the inlet. The downstream electrode area thus contributes significantly less to the overall performance of the reactor.

[a]*Department of Mechanical Science & Engineering, University of Illinois at Urbana-Champaign, 1206 W. Green St., Urbana, IL, 61801, USA*
[b]*Department of Chemical & Biomolecular Engineering, University of Illinois at Urbana-Champaign, 600 S. Mathews Ave, Urbana, IL, 61801, USA. E-mail: kenis@uiuc.edu*
† The HTML version of this article has been enhanced with additional colour images.

the formation of reaction-induced depletion boundary layers on the electrodes (Fig. 1a and b). For optimal performance, *i.e.* high conversion rates at the electrode, it is important to maximize the rate by which the concentration boundary layer at the electrodes gets replenished, while minimizing the extent of mixing at the liquid–liquid interface between the two streams. The diffusional mixing of adjacent streams in a microfluidic channel has been studied extensively, both experimentally and theoretically,[25–29] and typically does not limit the rate of a chemical process at the reactive surface, although it can have a detrimental effect on the overall conversion efficiency. Overcoming the mass-transfer limitations resulting from the presence of a depletion boundary layer on the reactive surface is key to improving the conversion efficiency.[21] Reducing the thickness of this depletion boundary layer (through an increase in the volumetric flow rate or a reduction of the channel diameter) will lead to increased mass transport since the diffusion distance will be shorter and the flux of diffusional transport to the surface will be higher as a result of the steeper concentration gradient. Unfortunately, with an increased linear velocity a smaller overall fraction of the reagents will have a chance to react due to the reduced residence time.

In this paper, we describe three different approaches to engineer the reaction-depletion boundary layer in order to reduce or even overcome mass transfer limitations of the desired process. The first two approaches involve the integration of multiple periodically-placed outlets along the reactive surface to remove the depleted zone and the integration of multiple periodically-placed inlets to add fresh reagents to the reactive surface. The third approach makes use of integrated herringbone ridges that produce a spiraling, transverse flow to enhance mass transfer of fresh reactant to the reactive surface while removing the depleted zone. These 'herringbone' ridges have been introduced earlier by Stroock *et al.* for micromixer applications.[30,31] For all three approaches to engineer depletion boundary layers, the design, fabrication, and characterization (*i.e.* quantification of the enhancement of mass transport achieved) will be discussed, supported by experimental data and simulations.

Experimental

Materials

The elastomer poly(dimethylsiloxane) or PDMS (Sylgard 184, Dow Corning, Midland, MI) was used to create many of the microfluidic devices used in this study. All experiments were performed with 18 MΩ Millipore water (E-pure, Barnstead, Dubuque, IA). All other chemicals were purchased from Sigma-Aldrich (St. Louis, MO).

Microfluidic devices for circuit model characterization

The master for fabrication of the microfluidic device in PDMS was obtained by standard photolithography[32] using negative photoresist (SU-8 50 from MicroChem Corporation, Newton, MA) and high resolution transparency films (5080 dpi, Herkules Image Setter) as the mask. The mask designs were created with CAD Software (Freehand 9, Macromedia, San Jose, CA). The positive relief features of the resulting master were 100 μm high and had various widths. Negative relief replicas in PDMS were obtained by replica molding,[32,33] yielding a replica of the master in PDMS with a microfluidic channel network embossed in negative relief in its surface. The microfluidic network was covered with a 5 mm thick polycarbonate sheet, and binder clips (OfficeMax, Shaker Heights, OH) were used to clamp this multi-layer assembly.

Microfluidic devices for performance characterization

The desired Y-shaped microreactor channel geometry was obtained by micromachining the desired channel design in either 250 or 500 μm thick polycarbonate sheets (Machine Shop, School of Chemical Sciences, University of Illinois). Next, the anodes and cathodes that line opposing sides on the inside of the main microfluidic channel, were deposited *via* sputtering of an adhesion layer of 50–100 Å of titanium followed by a layer of 500–1000 Å of gold. Finally, this polycarbonate membrane with Y-shaped microfluidic channel and integrated electrodes is sandwiched between 2 mm thick gasket layers of PDMS. This three-layer assembly was sandwiched between 5 mm thick polycarbonate sheets and held together using binder clips (OfficeMax, Shaker Heights, OH).

Microfluidic devices with integrated herringbone ridges

The master for fabrication of walls with herringbone ridges was obtained by standard photolithography.[32] The negative relief structure of the herringbone ridges was obtained in PDMS *via* replica molding.[32] Ridges with a height of 75 μm, a width of 250 μm, and a spacing of 250 μm were patterned in a 300 μm by 2.5 cm area at a $\sim 45^{\circ}$ angle with respect to the direction of flow. A 250 μm thick polycarbonate sheet with a 3 cm long and 250 μm wide Y-shaped microfluidic channel and integrated electrodes was aligned with the PDMS replica that contained the pattern of herringbone ridges using a microscope (Leica MZ12.5, Leica Microsystems, Wetzlar, Germany). A flat PDMS piece was placed on the other side of the polycarbonate membrane, and this three-layer assembly was sandwiched between 5 mm thick polycarbonate sheets, and held together using binder clips (OfficeMax, Shaker Heights, OH).

Circuit model characterization experiments

To perform the experiments to characterize the circuit model explained below, 18 MΩ Millipore water (E-pure, Barnstead, Dubuque, IA) was placed in 10 ml syringes, which were connected to the inlets of the microfluidic device using 16 gauge needles and polyethylene tubing (Intramedic, PE 205, ID = 1.57 mm). A syringe pump (Harvard Apparatus, PHD 2000) was used to introduce water at constant flow rates between 0.1 and 0.5 ml min^{-1}. Using the same tubing, water was collected from each of the six outlets in pre-weighed vials over eight-minute time intervals. To avoid gravity/siphoning effects, water was collected from the outlets in vials placed at the same height. The mass of the liquid was determined using a balance (ACCU-224, Fisher Scientific, Hampton, NH). Each experiment was repeated four times. For visualization of liquid removal at intermediate outlets, dyes were added to the

different inlet streams and optical micrographs were obtained using a stereomicroscope (Leica MZ12.5, Leica Microsystems, Wetzlar, Germany) equipped with a CCD video camera (Sony DXC-390).

Microreactor characterization experiments

The microreactors were characterized experimentally using a substrate stream of 5 mM of ferricyanide in 0.2 M KCl buffer solution and a stream of the same buffer solution without ferricyanide. Fluid flow in all experiments was pressure driven and regulated using a syringe pump (Harvard Apparatus, PHD 2000) with typical total flow rates between 0.1 and 0.5 ml min^{-1}. The experiments were run in potentiostatic mode using a potentiostat (PGSTAT 30, Autolab, Utrecht, The Netherlands). To control the potential of the cathode, a Pt wire was integrated as a reference electrode about 2 mm down from the inlet of the substrate stream, well before the streams merge in the stem of the Y-shaped channel. The conversion yield of ferricyanide to ferrocyanide was determined by measuring the amount of ferricyanide in the product stream after electroreduction using UV-vis spectroscopy as reported previously.[23]

Electrochemical microreactor simulations

To assess the performance of an example of a multistream laminar flow-based electrochemical microreactor, we simulated a laminar flow-based fuel cell (LFFC) using finite element method software FEMLAB 3.2 (Comsol, Stockholm, Sweden). The simulation was carried out by coupling the Navier–Stokes equation (eqn (1)), the continuity equation (eqn (2)), and the mass balance equation (eqn (3)) while using the Butler–Volmer equation (eqn (4), below) to simulate the oxidation of fuel (*e.g.* formic acid) at the anode.[34]

$$-\nabla\cdot\mu(\nabla\boldsymbol{u} + (\nabla\boldsymbol{u})^{\mathrm{T}}) + \rho(\boldsymbol{u}\cdot\nabla)\boldsymbol{u} + \nabla p = \boldsymbol{F} \quad (1)$$

$$\nabla\cdot\boldsymbol{u} = 0 \quad (2)$$

$$\nabla\cdot(-D\nabla c + c\boldsymbol{u}) = 0 \quad (3)$$

In these equations, μ is the viscosity, $\boldsymbol{u}$ the velocity, ρ the density, p the pressure, $\boldsymbol{F}$ the sum of the body forces, D the diffusion coefficient, and c the concentration. These equations were solved for the geometry as shown in Fig. 1b, with the x axis down the direction of flow, the y axis perpendicular to the direction of flow normal to the electrodes, and the z axis perpendicular to the direction of flow out of the plane. The diffusion coefficient (D, of formic acid) was set to 5×10^{-10} m^2 s^{-1}, the fluid density (ρ) to 1000 kg m^{-3}, and the fluid viscosity (μ) to 1×10^{-3} kg m^{-1} s^{-1}. For the Navier–Stokes equation, a flow rate of 0.1 to 0.8 ml min^{-1} per inlet and flow rates at each outlet defined by the pressure equaling zero were used. On all other surfaces the no-slip boundary condition was used.

To solve the mass balance equation, a concentration of 1 M of reactive species at the inlet of the substrate stream and a concentration of 0 at the inlet of the electrolyte stream were used. The electrochemical reaction on the anode was simulated with the Butler–Volmer equation (eqn (4)). Here, only the anode side was modeled since the performance of an air-breathing LFFC is typically limited by mass transport at the anode.[19,35]

$$J = \frac{i_0}{n_{\mathrm{tot}}F} \times \left[\frac{C_{\mathrm{O}}}{C_{\mathrm{O}}^*}\exp\left(\frac{\alpha n_{\mathrm{l}}F\eta}{RT}\right) - \frac{C_{\mathrm{R}}}{C_{\mathrm{R}}^*}\exp\left(-\frac{(1-\alpha)n_{\mathrm{l}}F\eta}{RT}\right)\right] \quad (4)$$

In this equation, i_0 is the exchange current density, n_{tot} is the number of total exchanged electrons, n_{l} is the number of electrons exchanged at the limiting rate step, C_{O} is the concentration of the oxidized form at the electrode, C_{O}^* is the bulk concentration of the oxidized form, C_{R} is the concentration of the reduced form at the electrode, C_{R}^* is the bulk concentration of the reduced form, α is the transfer coefficient, F is Faraday's constant, η is the overpotential, R is the gas constant, and T is the temperature.

Results and discussion

The Graetz problem in electrochemical microreactors

Steady-state diffusion-limited transport of chemical species to a reactive surface in a pressure-driven flow, known as the Graetz problem,[24] can be divided into two operation regimes: (*i*) an *entrance region* in which a reactant depletion boundary layer is formed and (*ii*) a *fully developed region* in which bulk depletion of the reagent occurs. The transition from the entrance region to the fully developed region is controlled by the ratio of length scales for diffusion and convection, expressed by the Graetz number, Gr, which equals $x\ w^{-1}\ \mathrm{Pe}^{-1}$, where the Péclet number, Pe, equals Uw/D, with x the length along channel, w the distance between electrodes, U the average linear velocity, and D the diffusivity.[24] For $\mathrm{Gr} < 1$, the convection timescale is shorter than the diffusion timescale and a portion of the reactant stream is not able to reach the electrode before leaving the channel (the entrance region). For $\mathrm{Gr} > 1$, reactants have plenty of time to reach the electrode and no concentration boundary layer develops. The electrochemical microreactors studied in this work are characterized by a high Pe, and thus a low Gr, which means that they operate in the entrance region. For example, in a LFFC operated at an overall linear flow rate U of 0.833 mm s^{-1}, with $w = 2$ mm, $D = 5 \times 10^{-10}$, and $x = 2.5$ cm, the Graetz number is 3.78×10^{-3}, which is significantly smaller than 1.

The performance of a microreactor that operates in the *entrance region* could be enhanced by engineering the reaction-depletion boundary layers such that mass transport of the reagents to the surface is enhanced. To reduce the boundary layer thickness one can increase the linear velocity either by increasing the volumetric flow rate or by reducing the electrode-to-electrode distance. With increasing linear velocity, a higher absolute amount of reactant will react at the electrode (steeper gradient and thus higher flux in a thinner boundary layer), but a smaller overall fraction of the reagents has a chance to react. The 'reactant utilization' could be increased by recirculation of the fluid stream, but diffusion of reactants away from the electrode and the reverse reaction at the counter electrode hamper this method. Here we report microfluidic designs that avoid the need for recirculation by periodically

replenishing or removing the depleted boundary layer, or by integration of structural elements, *i.e.* ridges, that induce a spiraling, transverse flow of fresh reactants towards the electrode surface.

The most elementary design of a laminar-flow based electrochemical microreactor consists of two inlets and one outlet (Fig. 1). When the reaction at the electrode is mass transfer limited, the electrode surface area is not efficiently utilized due to the concentration boundary layer growing from the electrode edge at the inlet (Fig. 1a). A simulation of the current density on the electrode surface shows that most of the reaction occurs close to the end of the electrode where the reactant stream enters (Fig. 1c).

To overcome mass transfer limitations as a result of the formation of reagent depletion boundary layers, we have created three microfluidic designs that remove and/or replenish the depleted boundary layer. In the first design, shown in Fig. 2a, the depleted layer of solution is removed periodically through multiple outlets, exposing the electrode surface to solution containing reactants at the initial concentration. In the second design, shown in Fig. 2b, multiple streams with reactants at the initial concentration are introduced periodically through multiple inlets along the electrodes, thereby pushing any depleted solution away from the surface. In the third design, shown in Fig. 2c, so-called herringbone ridges induce a flow transverse to the net direction of fluid flow as described previously by Stroock *et al.* for micromixer applications.[30] The depleted boundary layer is continuously replaced with solution from the middle of the channel, which contains reagent at a higher concentration.

Multiple outlets: circuit analysis for pressure balancing

Operation of microfluidic designs with multiple outlets or inlets requires accurate control of volumetric flow rates through each segment of the fluidic network to ensure that exactly the desired fraction of the depletion boundary layer is removed or that exactly the desired amount of new solution is introduced periodically. The volumetric flow in each segment of a network of channels depends on the relative magnitude of the fluidic resistance of all segments, which in turn depends on the length and area of each segment. To accurately control volumetric flow rates, pressure balancing is required, since the pressure drop of a segment is the product of the volumetric flow rate and its fluidic resistance ($\Delta p = Q \times R$). Pressure balancing can be achieved by performing a circuit analysis of fluidic resistances, analogous to a circuit analysis of electrical or thermal resistances.[36]

For the multi-outlet design (Fig. 2a), the thickness of the boundary layer that needs to be removed at successive outlets can be determined using a boundary layer analysis.[37] The thickness of a concentration boundary layer scales as follows: $\delta_c \sim \mathrm{Sc}^{1/3}\, x\, \mathrm{Re}_x^{-1/2}$, where the Schmidt number Sc equals $\mu/\rho D$, with μ the viscosity, D the diffusivity, and x the length along the channel, and the local Reynolds number Re_x equals $\rho\, x\, U/\mu$. Then, the volumetric flow rate of the depleted zone to be removed, as a function of position away from the surface (y) and distance down the channel (x) can be calculated by integrating the velocity profile equation (eqn (5)) where Δp is the pressure drop, w is the width of the channel, μ is the viscosity, L is the length of the channel, h is the height of the channel, and x, y, and z are the coordinates of the channel.

$$v_x(y,z) = -\frac{\Delta p w^2}{8\mu L}\left\{1-\left(\frac{2y}{w}\right)^2 + \frac{32}{\pi^3}\sum_{n=1}^{\infty} B_n \cosh\left[\frac{(2n-1)\pi z}{w}\right]\cos\left[\frac{(2n-1)\pi n}{w}\right]\right\} \quad (5)$$

$$\text{with } B_n = \frac{(-1)^n}{(2n-1)^3}\left\{\cosh\left[\frac{(2n-1)\pi R}{2}\right]\right\}^{-1} \quad (5a)$$

$$\text{and } R = h/w \quad (5b)$$

After the volumetric flow rates for all segments in the fluidic network are determined, control of the relative volumetric flow through each segment is achieved by balancing the pressure across the various segments of the microfluidic network, which is implemented through a circuit analysis of fluidic resistances. Fig. 3 shows the design of a fluidic network with multiple outlets, with each segment labeled with a volumetric flow rate Q and a fluidic resistance R. In general, in a fluidic network,

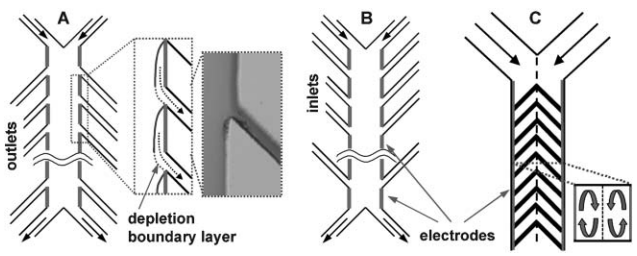

Fig. 2 Three approaches to improve mass transport of reactants to reactive surfaces, such as electrodes. (A) Multiple outlet design to periodically remove the depleted zone. Inset: Optical micrograph of removal of a dyed stream. (B) Multiple inlet design to supply periodically fresh reactants to the surface. (C) Microreactor with integrated herringbone ridges to create a spiraling, transverse flow (see inset) to remove the depleted layer while supplying solution with fresh reactant from the middle of the channel.

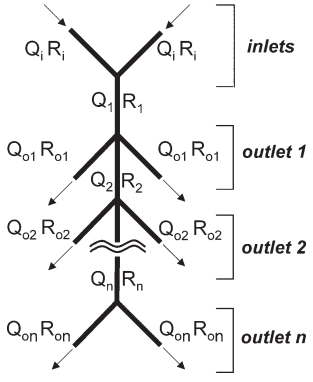

Fig. 3 Schematic representation of a fluidic network with two inlets and multiple outlets with volumetric flow rates Q_i and fluidic resistances R_i for each inlet i, each main channel section 1, 2,…, n, and each outlet o1, o2,…, on.

the pressure drop is related to the fluidic resistance and the flow rate according to eqn (6), where Δp is the pressure drop, Q is the flow rate, and R is the fluidic resistance. The individual fluidic resistance in each segment of the network is calculated using the resistance equation (eqn (7)), which holds for rectangular channels with low aspect ratios.[38] The fluidic resistance for a high aspect ratio channel can be approximated with eqn (8), since $h/w \rightarrow 0$.

$$\Delta p = QR \tag{6}$$

$$R = \frac{12\mu L}{wh^3}\left[1 - \frac{h}{w}\left(\frac{192}{\pi^5}\sum_{n=1}^{\infty}\frac{1}{n^5}\tanh\left(\frac{n\pi w}{h}\right)\right)\right]^{-1} \tag{7}$$

$$\text{For } h/w \rightarrow 0 \qquad R = \frac{12\mu L}{wh^3} \tag{8}$$

Since the fluid is introduced through a single inlet and flows out to ambient air through multiple outlets, the pressure drops between the inlet and each outlet are identical. The volumetric flow rate at the inlet is set by a syringe pump and the other volumetric flow rates through each channel segment within the fluidic network are calculated by integrating the velocity profile (eqn (5)). From eqn (9), we calculate the ratios between resistances (R_{I}, R_{II}, R_{III},…), where R_{I} is the total resistance between the inlet and the end of first outlet, R_{II} is the total resistance between the inlet and the end of the second outlet, and so on (Fig. 3).

$$\Delta p_{\mathrm{I}} = Q_{\mathrm{I}}R_{\mathrm{I}} = Q_{\mathrm{II}}R_{\mathrm{II}} = Q_{\mathrm{III}}R_{\mathrm{III}} = \ldots\ldots = Q_nR_n \tag{9}$$

$$\text{where} \qquad R_{\mathrm{I}} = \frac{R_i}{2} + R_1 + \frac{1}{\frac{2}{R_{\mathrm{o1}}} + \frac{1}{R_{\mathrm{II}}}} \tag{9a}$$

$$R_{\mathrm{II}} = R_2 + \frac{1}{\frac{2}{R_{\mathrm{o2}}} + \frac{1}{R_{\mathrm{III}}}} \tag{9b}$$

$$R_{\mathrm{III}} = R_3 + \frac{1}{\frac{2}{R_{\mathrm{o3}}} + \frac{1}{R_{\mathrm{IV}}}} \tag{9c}$$

$$\text{or in general for the } n^{\mathrm{th}} \text{ outlet}: R_{\mathrm{I}(n)} = R_n + \frac{1}{\frac{2}{R_{\mathrm{o}n}} + \frac{1}{R_{\mathrm{I}(n+1)}}} \tag{9d}$$

After the resistances of all the segments in the fluidic network are calculated, the dimensions of the intermediate outlet channels can be determined with eqn (10).

$$L = \frac{wh^3R}{12\mu}\left[1 - \frac{h}{w}\left(\frac{192}{\pi^5}\sum_{n=1}^{\infty}\frac{1}{n^5}\tanh\left(\frac{n\pi w}{h}\right)\right)\right] \tag{10}$$

To characterize the accuracy of the circuit analysis of fluidic resistances, we fabricated and tested two microfluidic devices with three outlets on each side, but with two different designs for the main channel: one with a tapered main channel and one with a main channel of constant width. The advantage of a tapered main channel design is that the average linear velocity in the main channel can be kept constant even after depleted zones are removed at intermediate outlets.

The procedure to design a microreactor with multiple outlets in which an exact amount of the depletion boundary layer is removed thus can be summarized as follows:

Step 1. Choose appropriate independent dimensions for the different segments in the fluidic network: all widths, heights, and lengths for the inlets and the main channel, and the widths and heights, but not the lengths for all outlets.

Step 2. Calculate the volumetric flow rates of the depleted zones to be removed at intermediate outlets by integrating the velocity equation (eqn (5)).

Step 3. Calculate the fluidic resistances of each segment in the fluidic network (eqn (8) and (9)).

Step 4. Calculate the appropriate channel length for each outlet (eqn (10)).

We chose a set of dimensions as listed in Table 1, based on a typical design of laminar flow-based electrochemical microreactors, *i.e.* LFFCs[19–21] or microreactors for cofactor regeneration.[23] Different dimensions can also be chosen, as long as the lengths of the outlet channels are adjusted to ensure that the appropriate fraction of the depletion boundary layer is removed under the operating conditions used. We calculated the volumetric flow rates of the depleted zones to be removed at consecutive outlets by integrating the velocity equation (eqn (5)) using boundary layer thicknesses of 50 and 80 μm, which we selected based on typical boundary layer thicknesses encountered in simulations such as those shown in Fig. 1. Next, we calculated the fluidic resistances of each segment in the network with eqn (8) and (9). Finally, the lengths of the

Table 1 Dimensions of microreactors with multiple outlets capable of removing a depletion boundary layer of certain width (here 80 μm) at consecutive outlets

		Tapered channel	Constant channel width
Independent parameters	Height of device	100 μm	100 μm
	Width of main channel	500, 431, 353 μm[a]	500 μm
	Length of main channel	30 mm	30 mm
	Widths of inlet and last outlet	500 μm	500 μm
	Lengths of inlet and last outlet	10 mm	10 mm
	Width of intermediate outlets	90 μm	90 μm
	Spacing between outlets	10 mm	10 mm
	Thickness of layer removed at intermediate outlets	80 μm	80 μm
Calculated with eqn (10)	Length of outlet 1	24.81 mm	21.51 mm
	Length of outlet 2	12.67 mm	14.78 mm

[a] The consecutive main-channel widths in this tapered channel design were chosen so that the average linear velocity in the main channel remains constant after the removal of a fluid layer at each outlet.

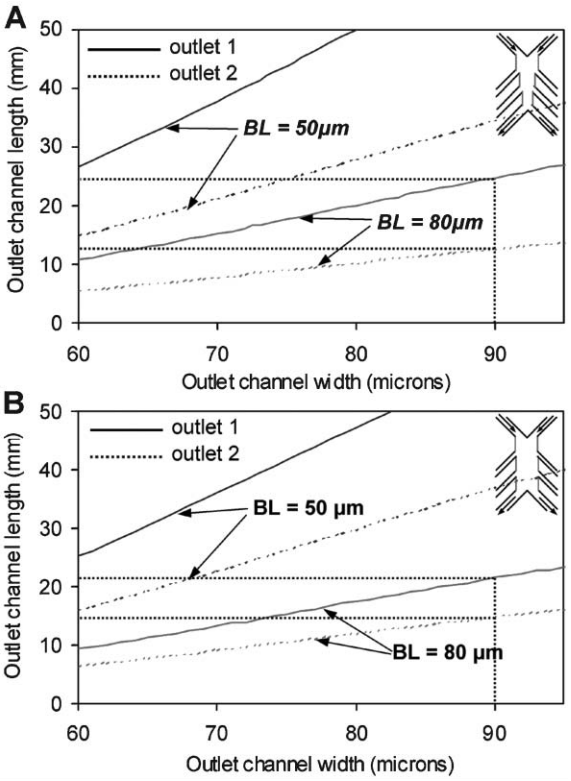

Fig. 4 Engineering chart to determine appropriate combinations of outlet channel length and width to remove a depletion boundary layer (BL) of certain thickness. The lines plotted here are for BL thicknesses of 50 and 80 μm, which are removed at these outlets for a design with a tapered main channel (A), or with a main channel of constant width (B). The dotted horizontal and vertical lines indicate an example of a combination of dimensions that will exactly remove an 80 μm BL at the first and second outlet.

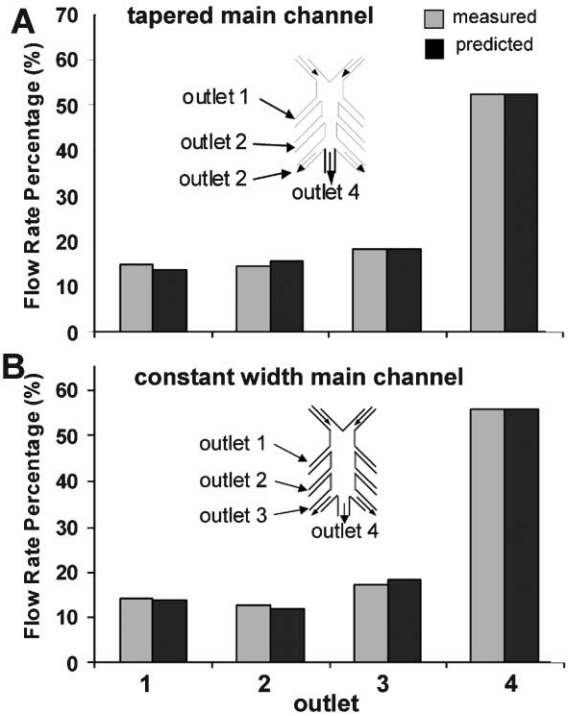

Fig. 5 Comparison of volumetric flow rates experimentally measured at consecutive outlets and volumetric flow rates attained from analytical calculations for a multi-outlet microreactor design (A) with a tapered main channel; and (B) with a constant main channel width. This result shows that circuit analysis of the fluidic network to balance pressure drops works well for this application. Error: ±8% of measured values.

intermediate outlets were calculated with eqn (10). Fig. 4 shows an engineering design chart from which appropriate combinations of outlet channel widths and lengths can be determined for different depleted boundary layer thicknesses to be removed. Fig. 4a shows this for a design with a tapered main channel and Fig. 4b for a design with a main channel of constant width. Given that we chose outlet channels that were 90 μm wide, the lengths required for the first and second outlets can be read off the chart by following the vertical and horizontal dotted lines. In Fig. 4, only sets of lines for two boundary layer thicknesses to be removed are plotted, but using eqn (10), lines for other boundary layer thicknesses to be removed for the same or other chosen fluidic network dimensions can be plotted.

To validate the circuit analysis for these multi-outlet fluidic networks we picked two sets of dimensions, one for a tapered channel design and one for a design with constant channel width, and using Fig. 4 or eqn (10), the appropriate lengths for the different outlets were determined (Table 1). After fabrication of these two microfluidic networks, we quantified the volumetric flow rates through each outlet by weighing the mass collected at each outlet. Fig. 5 shows excellent agreement between the experimental flow rate ratios at the outlets and the corresponding theoretical flow rate ratios. The agreement between experiment and theory demonstrates that circuit analysis of microfluidic networks is sufficently accurate to create design rules and engineering design charts such as those reported here for the periodic removal of reaction depletion boundary layers of certain thickness.

Multiple outlets microreactor: simulation

We also investigated the performance of electrochemical microreactors with multiple outlets by finite element methods implemented in FEMLAB (Comsol, Stockholm, Sweden). This simulation was carried out by coupling the Navier–Stokes equation, the continuity equation, the mass balance equation, and, as a boundary condition at the electrode, the Butler–Volmer equation, as explained in detail in the experimental section above.

As an example of an electrochemical microreactor that would benefit from enhancement of mass transport at the electrode, we chose the laminar flow-based fuel cell (LFFC) that we introduced a few years ago.[19–21,35,39] This microfuel cell design utilizes the occurrence of laminar flow in microfluidic channels to achieve the necessary compartmentalization of the fuel and oxidant streams in a single channel without a physical barrier such as the commonly used membrane electrolyte assembly (MEA). An aqueous stream containing a liquid fuel, *e.g.* formic acid, methanol, or dissolved hydrogen, and an aqueous electrolyte stream are introduced into a single microfluidic channel and the lack of turbulent

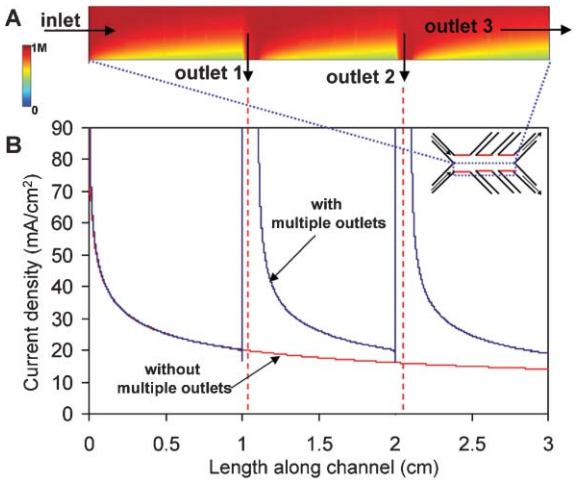

Fig. 6 (A) Simulated concentration profile of a 1 M formic acid stream reacting at a segmented anode in laminar flow fuel cell. The depletion boundary layers that develop on the electrode from the leading edge are periodically removed at the three outlets. (B) Current density as a result of formic acid oxidation at the center of the anode *vs.* length along the channel *with* and *without* multiple outlets, clearly showing the benefit of the periodic removal of depleted fluid layers.

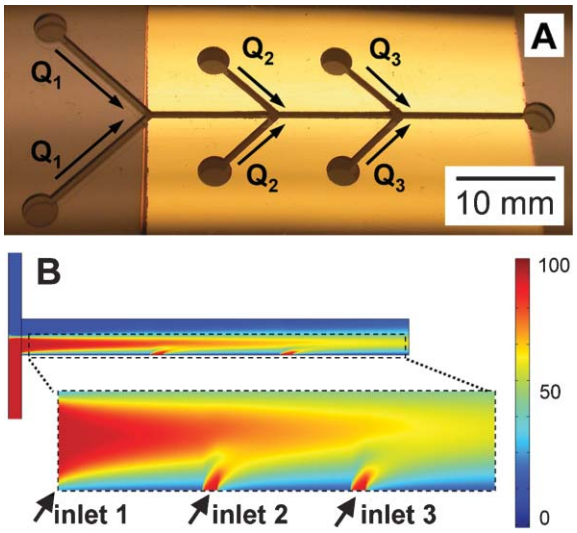

Fig. 7 (A) Optical micrograph of a microreactor fabricated in a polycarbonate sheet with three inlets along each electrode. (B) Simulated concentration profile (arbitrary units) of ferricyanide being reduced at the cathode in this reactor while introduced through multiple inlets.

mixing keeps the two streams localized on, respectively, the anode and cathode.[19–21,35,39]

Fig. 6a shows a simulated concentration profile of a LFFC with three outlets, operated with 1 M formic acid as the fuel. The reaction depletion boundary layers form from the leading edge of the anode and are removed at periodically-placed outlets that are 1 cm apart. Every time the boundary layer is removed at an outlet, the current density on the electrode recovers to the value of that at the inlet (Fig. 6b). Overall, a higher current density and thus more current is generated over the length of the electrode when multiple outlets are present. Depending on the flow rate (typically between 0.1–0.8 ml min^{-1}), a 30 to 100% increase in current density can be obtained for the laminar flow fuel cell simulated here.

Multiple inlet microreactor: simulation and experiment

Next we characterized a microreactor design with three inlets placed periodically along each electrode (Fig. 7a). In contrast to the design with three outlets along each electrode, the multi-inlet design increases mass transport to the electrodes by periodically pushing the depleted boundary layer away from the electrode surface with a fresh stream of reagents. Fig. 7b shows a simulated concentration profile of ferricyanide in a three-inlet microreactor. As fresh reagents are introduced at the intermediate inlets the depleted layer is pushed away and a new boundary layer is formed. For comparison, the concentration profile without the additional inlets (*i.e.* single inlet) would look similar to the simulation shown in Fig. 1b.

We also studied the performance of this reactor experimentally using the ferricyanide/ferrocyanide redox couple as a model system. An appropriate network of 500 μm wide channels was machined in a 500 μm thick polycarbonate sheet, and gold (Au) electrodes were deposited *via* shadow-sputtering (Fig. 7). The microreactor was run in a potentiostatic mode at −0.1 V *vs.* a Pt electrode placed in the cathodic stream near the inlet of the first Y-junction. To unravel the beneficial effects of having multiple inlets along the electrodes, we performed the following three experiments (Table 2). In the first experiment, a buffer stream and a substrate stream containing 5 mM ferricyanide in the same buffer were introduced through the first set of inlets only, so Q_1 = 0.05 ml min^{-1} per inlet and Q_2 = Q_3 = 0. The ferricyanide is reduced at the cathode, while the oxidation of water occurs at the anode. This first experiment is the equivalent of a microreactor that lacks additional inlets along the electrodes. In a second experiment, reactant streams are introduced through all three inlets: Q_1 = 0.05 ml min^{-1} per inlet and Q_2 = Q_3 = 0.01 ml min^{-1} per inlet. Introducing three additional feeds of reactants at the inlets 2 and 3 resulted in a 56% increase of current density, from 64.6 to 100.4 μA (Table 2), compared to the experiment with only the inlets 1 being used.

One additional experiment needs to be performed, however, since the total flow rate in the second experiment increased from 0.05 to 0.07 ml min^{-1} with the introduction of the additional two reactant streams along the electrodes. A higher flow rate is expected to increase the mass transfer coefficient (thinner depletion boundary layer), but the question is by how

Table 2 Comparison of the performance of an electrochemical microreactor with multiple inlets operated in three different ways

Experiment		Q_1/ml min^{-1}	Q_2/ml min^{-1}	Q_3/ml min^{-1}	Current/μA
1	Inlet 1 only	0.05	0	0	64.6
2	Inlet 1 only	0.07	0	0	75.0
3	Inlets 1, 2 & 3	0.05	0.01	0.01	100.4

much compared to the expected increase of mass transfer as a result of the additional inlets. So, in the third experiment, the reactant streams were only provided through the first set of inlets (no. 1), but now with a total flow rate of $Q_1 + Q_2 + Q_3 =$ 0.07 ml min^{-1}. This experiment verified that the increase of current density from the first to the second experiment was mostly due to addition of fresh reactants from the additional inlets along the electrodes rather than due to a flow rate-induced increase of the mass transfer coefficient. Indeed, upon increasing the flow rate from 0.05 ml min^{-1} in the first experiment to 0.07 ml min^{-1} in the third experiment, the current density increased, but by only 15%, from 64.6 to 75.0 μA. Therefore, the rest of the increase in current density observed in the second experiment in which all inlets along the electrode are used can be attributed to the beneficial effect of periodically supplying fresh reactant along the electrode.

Integrated herringbone ridges to induce transverse flow

Another method to increase mass transfer of reagents to the electrode is by integrating ridges that introduce transverse flow (Fig. 1C). The herringbone mixer, as reported Stroock *et al.*,[30,31] is a chaotic mixer for continuous flow systems wherein ridges patterned like herringbones at 45° angles on a channel wall induce a secondary transverse, spiraling flow through part of or the whole channel. This configuration efficiently mixes fluid inside a microchannel by stretching and folding two or more streams that enter a microfluidic channel in laminar flow. Inter-diffusional mixing between the streams is enhanced once they are stretched in thinner sheets that are wrapped around each other.

In this work, the purpose of using the herringbone ridges is not to mix the reagents present in different streams inside the microchannel. Instead, we wished to enhance transport of reagents from the middle of the channel to the electrode by a secondary transverse flow. We integrated asymmetric 'herringbone' ridges along one channel wall. Appropriate placement of the ridges will induce a folding of the reactant stream so reactants initially present at the middle of the microfluidic channel will spiral towards the electrode surface further downstream. The integrated ridges thus enable continuous replacement of the depleted boundary layers on the electrode with solution containing reactant, thereby increasing both the net conversion rate as well as the reactant utilization efficiency.

We fabricated a 3 cm long Y-shaped microreactor with a herringbone ridges pattern on the bottom wall of a 250 μm × 250 μm channel containing Au electrodes on opposing side walls (see Experimental). Just as for the multi-inlet microreactors, we used the ferricyanide/ferrocyanide redox couple as a model system to show the promise of this method of mass transfer enhancement in microreactors. In a first experiment, a buffer stream and a substrate stream containing ferricyanide in the same buffer solution were introduced in laminar flow into an identical microreactor *without* integrated ridges. In a second experiment, we did the same in a microreactor *with* integrated ridges across the width of the channel beginning from 1 cm downstream from the inlet. Fig. 8 shows the conversion of ferricyanide as a function of total flow rate for two different flow rate ratios between the substrate stream and the buffer

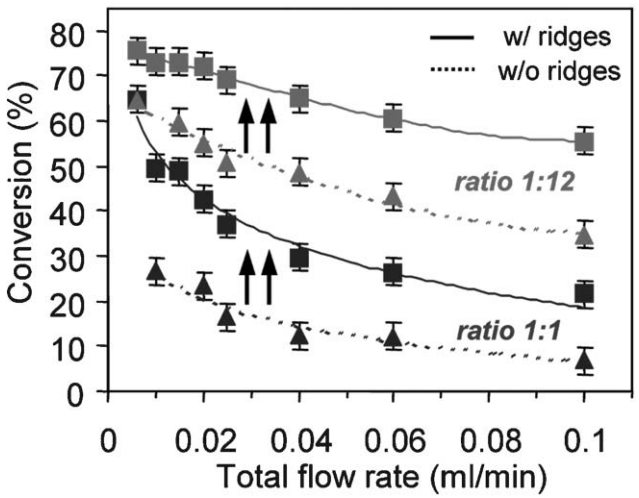

Fig. 8 Experimentally measured ferricyanide conversion as a function of total flow rate in electrochemical microreactors with and without integrated herringbone ridges, operated at cathodic over anodic stream flow rate ratios of 1 : 1 or 1 : 12. Error: 3% of measured values.

stream, for both the microreactor with and without integrated ridges. As expected for both microreactors, the conversion increases for lower total flow rates and for higher flow rate ratio.[23] At a substrate-to-buffer flow rate ratio of 1 : 1, a large fraction of the substrate leaves the microreactor without reacting, whereas at a ratio of 1 : 12 most of the substrate reacts at the electrode. While both microreactors exhibited the same trends as a function of total flow rate and substrate-to-buffer flow rate ratio, the conversion efficiency increased by anywhere from 10 to 40% when using the microreactor with integrated ridges (Fig. 8). Comparison of these two experiments clearly shows that the integration of ridges in one of the channel walls enhanced mass transport of unreacted ferricyanide to the electrode. A maximum conversion efficiency of close to 76% was obtained when running the microreactor with integrated grooves at a total flow rate of 6 μl min^{-1} and a substrate-to-buffer flow rate ratio of 1 : 12.

Discussion and conclusion

The performance of multistream laminar flow-based microreactors that rely on surface reactions such as LFFCs, is typically limited by mass transfer due to the formation of a reaction depletion boundary layer. This paper introduced three methods to engineer a depletion boundary layer such that the transport rate of the reactants to the surface is enhanced: (*i*) removing the depleted zone through multiple periodically-placed outlets; (*ii*) adding fresh reactants to the surface through multiple periodically-placed inlets; or (*iii*) producing a spiraling, transverse flow through integration of ridges along a channel wall.

The performance of the microreactors, reactant conversion at the electrodes, could be increased by anywhere from 10 to 100% using these different methods to enhance mass transfer described here. In principle, one could place even more inlets or outlets along each electrode, but soon one encounters the trade-off between an increase in conversion efficiency and an

overly complex fluidic system (higher pressure drops), as well as consumption of electrode area by the area needed for additional inlets or outlets. To improve the reactant conversion rate, approaches (*i*) and (*ii*) are most appropriate to use since these approaches remove depletion boundary layers and do not use the depleted zone again, thereby maintaining a high reactant concentration near the electrode. On the other hand, to improve the reactant conversion efficiency (*i.e.* reactant utilization), approach (*iii*) is appropriate since this approach not only removes the depletion boundary layer, but also recycles the un-depleted zone from the middle of the channel to the electrode surface.

In terms of design and fabrication of a microreactor that relies on surface chemistries, approaches (*i*) and (*ii*) require more space than approach (*iii*), but the fabrication will be simpler because approaches (*i*) and (*ii*) have a single-height design whereas approach (*iii*) has a design with features of multiple heights. Recently, however, Toepke *et al.* showed that multilevel features can be formed in a single step using a new method that makes use of the diffraction of light in a single exposure photolithographic procedure, thereby allowing rapid fabrication of multilevel microfluidic channel designs as required for the third approach.[40] During operation, approaches (*i*) and (*ii*) will require more energy for fluidic pumping than approach (*iii*) because they have a more complex fluidic network with narrower fluidic channels (higher overall pressure drop), whereas approach (*iii*) operates in a single, wider channel.

Depending on the purpose and/or the size of an application, access to fabrication tools, and/or the capabilities of a pump, one of the discussed approaches can be chosen to improve the performance of a microfluidic reactor operating in a laminar flow regime in which the performance typically relies on efficient mass transfer of reactant to the reactive surface, such as an electrode.

Acknowledgements

This work was funded by the University of Illinois. The authors thank Michael Mitchell for stimulating discussions. Financial support by the University of Illinois and by NSF-CTS for a CAREER award to PJAK is gratefully acknowledged.

References

1 K. F. Jensen, *Chem. Eng. Sci.*, 2001, **56**, 293–303.
2 L. R. Arana, S. B. Schaevitz, A. J. Franz, M. A. Schmidt and K. F. Jensen, *J. Microelectromech. Syst.*, 2003, **12**, 600–612.
3 O. Reynolds, *Philos. Trans. R. Soc. London, Ser. A*, 1886, **177**, 157–233.
4 W. Ehrfeld, K. Golbig, V. Hessel, H. Lowe and T. Richter, *Ind. Eng. Chem. Res.*, 1999, **38**, 1075–1082.
5 M. A. Burns, B. N. Johnson, S. N. Brahmasandra, K. Handique, J. R. Webster, M. Krishnan, T. S. Sammarco, P. M. Man, D. Jones, D. Heldsinger, C. H. Mastrangelo and D. T. Burke, *Science*, 1998, **282**, 484–487.
6 E. T. Lagally, C. A. Emrich and R. A. Mathies, *Lab Chip*, 2001, **1**, 102–107.
7 E. T. Lagally, I. Medintz and R. A. Mathies, *Anal. Chem.*, 2001, **73**, 565–570.
8 E. T. Lagally, P. C. Simpson and R. A. Mathies, *Sens. Actuators, B*, 2000, **63**, 138–146.
9 P. D. I. Fletcher, S. J. Haswell, E. Pombo-Villar, B. H. Warrington, P. Watts, S. Y. F. Wong and X. L. Zhang, *Tetrahedron*, 2002, **58**, 4735–4757.
10 S. K. W. Dertinger, D. T. Chiu, N. L. Jeon and G. M. Whitesides, *Anal. Chem.*, 2001, **73**, 1240–1246.
11 N. L. Jeon, S. K. W. Dertinger, D. T. Chiu, I. S. Choi, A. D. Stroock and G. M. Whitesides, *Langmuir*, 2000, **16**, 8311–8316.
12 C. L. Hansen, E. Skordalakes, J. M. Berger and S. R. Quake, *Proc. Natl. Acad. Sci. U. S. A.*, 2002, **99**, 16531–16536.
13 R. C. Gunawan, E. R. Choban, J. E. Conour, J. Silvestre, L. B. Schook, H. R. Gaskins, D. E. Leckband and P. J. A. Kenis, *Langmuir*, 2005, **21**, 3061–3068.
14 H. B. Mao, P. S. Cremer and M. D. Manson, *Proc. Natl. Acad. Sci. U. S. A.*, 2003, **100**, 5449–5454.
15 E. M. Lucchetta, M. S. Munson and R. F. Ismagilov, *Lab Chip*, 2006, **6**, 185–190.
16 E. M. Lucchetta, J. H. Lee, L. A. Fu, N. H. Patel and R. F. Ismagilov, *Nature*, 2005, **434**, 1134–1138.
17 B. H. Weigl and P. Yager, *Science*, 1999, **283**, 346–347.
18 J. P. Brody and P. Yager, *Sens. Actuators, A*, 1997, **58**, 13–18.
19 R. S. Jayashree, L. Gancs, E. R. Choban, A. Primak, D. Natarajan, L. J. Markoski and P. J. A. Kenis, *J. Am. Chem. Soc.*, 2005, **127**, 16758–16759.
20 E. R. Choban, J. S. Spendelow, L. Gancs, A. Wieckowski and P. J. A. Kenis, *Electrochim. Acta*, 2005, **50**, 5390–5398.
21 E. R. Choban, L. J. Markoski, A. Wieckowski and P. J. A. Kenis, *J. Power Sources*, 2004, **128**, 54–60.
22 D. Erickson, X. Z. Liu, U. Krull and D. Q. Li, *Anal. Chem.*, 2004, **76**, 7269–7277.
23 S. K. Yoon, E. R. Choban, C. Kane, T. Tzedakis and P. J. A. Kenis, *J. Am. Chem. Soc.*, 2005, **127**, 10466–10467.
24 T. Gervais and K. F. Jensen, *Chem. Eng. Sci.*, 2006, **61**, 1102–1121.
25 R. F. Ismagilov, A. D. Stroock, P. J. A. Kenis, G. Whitesides and H. A. Stone, *Appl. Phys. Lett.*, 2000, **76**, 2376–2378.
26 A. E. Kamholz and P. Yager, *Sens. Actuators, B*, 2002, **82**, 117–121.
27 A. E. Kamholz, E. A. Schilling and P. Yager, *Biophys. J.*, 2001, **80**, 1967–1972.
28 A. E. Kamholz and P. Yager, *Biophys. J.*, 2001, **80**, 155–160.
29 A. E. Kamholz, B. H. Weigl, B. A. Finlayson and P. Yager, *Anal. Chem.*, 1999, **71**, 5340–5347.
30 A. D. Stroock, S. K. W. Dertinger, A. Ajdari, I. Mezic, H. A. Stone and G. M. Whitesides, *Science*, 2002, **295**, 647–651.
31 A. D. Stroock, S. K. Dertinger, G. M. Whitesides and A. Ajdari, *Anal. Chem.*, 2002, **74**, 5306–5312.
32 D. C. Duffy, J. C. McDonald, O. J. A. Schueller and G. M. Whitesides, *Anal. Chem.*, 1998, **70**, 4974–4984.
33 J. C. McDonald, D. C. Duffy, J. R. Anderson, D. T. Chiu, H. K. Wu, O. J. A. Schueller and G. M. Whitesides, *Electrophoresis*, 2000, **21**, 27–40.
34 G. Prentice, *Electrochemical Engineering Principles*, Prentice Hall, Upper Saddle River, NJ, 1991.
35 R. S. Jayashree, D. Egas, J. S. Spendelow, D. Natarajan, L. J. Markoski and P. J. A. Kenis, *Electrochem. Solid-State Lett.*, 2006, **9**, A252–A256.
36 F. P. Incropera and D. P. Dewitt, *Fundamentals of Heat and Mass Transfer*, John Wiley & Sons, New York, 2002.
37 R. B. Bird, W. E. Stewart and E. N. Lightfoot, *Transport Phenomena*, Wiley, New York, 2nd edn, 2002.
38 G. T. A. Kovacs, *Micromachined Transducers Sourcebook*, McGraw-Hill, New York, 1998.
39 E. R. Choban, P. Waszczuk and P. J. A. Kenis, *Electrochem. Solid-State Lett.*, 2005, **8**, A348–A352.
40 M. W. Toepke and P. J. A. Kenis, *J. Am. Chem. Soc.*, 2005, **127**, 7674–7675.

